LROC NAC DIGITAL TERRAIN MODEL (DTM) PRODUCTION. M. R. Henriksen[1], M. R. Manheim[1], E. J. Speyerer[1], A.K. Boyd[1], and M. S. Robinson[1], [1]School of Earth and Space Exploration, Arizona State University, 1100 S. Cady, Tempe, AZ 85287 – (mhenriksen@ser.asu.edu)

Introduction: Lunar Reconnaissance Orbiter Camera (LROC) Narrow Angle Camera (NAC) stereo observations combined with Lunar Orbiter Laser Altimeter (LOLA) profiles provide the inputs required to create dense and accurate DTMs of the lunar surface. The NACs consist of two linear pushbroom cameras designed to collect 0.5 m pixel scale images with a combined swath of 5 km at an altitude of 50 km [1]. The LROC Operations Team acquires stereo pairs on two separate orbits, where the spacecraft is slewed off-nadir for at least one orbit. The convergence angle between the two images has a range of 10° to 40°. LOLA altimeter profiles with GRAIL gravity model improvements are accurate to within 10 meters horizontally and 1 m radially [2]. We use multiple LOLA profiles to improve and evaluate the absolute accuracy of each NAC DTM.

Methodology: DTM processing at ASU is completed using a combination of the Integrated Software for Imagers and Spectrometers (ISIS) and SOCET SET from BAE Systems [3].

Pre-processing. We first ingest, radiometrically calibrate, and remove echo effects using ISIS [4] for each image collected as part of the stereo observation. ISIS is used to apply orientation parameters stored in a series of Spacecraft, Planet, Instrument, C-Matrix and Events (SPICE) kernels. These parameters are then formatted for compatibility and imported into SOCET SET [5].

Relative Orientation. To register the images to the geodetically accurate LOLA grid [2], each image is first corrected for relative orientation to the other images in the stereo model [6]. First, a set of "tie" points are inserted by matching pixels between images, which are then aligned using a multi-sensor triangulation (MST) algorithm [7,8]. Once an acceptable RMS error (<0.5 pixels) is reached for the stereo model, a first-iteration DTM is extracted for absolute registration.

Absolute Orientation. We developed an automated tool using the Optimization Toolbox within MATLAB [9] to register multiple altimeter profiles from LOLA to the initial DTM. These registered coordinates are then exported back to SOCET SET as control points. We perform a final bundle adjustment to improve the absolute positioning of the NAC images. In addition to assessing the overall RMS error and point residuals for the solution, we evaluate the latitude, longitude, and elevation RMS errors based on LOLA profile accuracies.

Terrain Extraction. The Next Generation Automatic Terrain Extraction (NGATE) program in SOCET SET is used to extract elevation values from the epipolar rectified images [6,8] using image correlation and edge matching algorithms on each image pixel [9,10]. The DTM is then resampled to at least three times the ground sampling distance (GSD) of the input images to reduce noise, typically at 2 or 5 m pixel scale. Next, the DTM is run through a single pass of the Adaptive Automatic Terrain Extraction (ATE) SOCET SET application, smoothing elevation data through image correlation in a single pass on individual posts rather than at each image pixel [11].

Orthophoto Generation. Once the DTM is processed, we create orthophotos, or orthorectified maps, of the original NAC images, at both the native image resolution and at the resolution of the DTM. The orthorectification process removes distortion due to camera obliquity and terrain relief [12].

Post-processing. For each set of stereo images, SOCET SET outputs the final DTM and confidence map as raw image files and the orthorectified images as 16-bit GeoTIFFs, which are imported into ISIS, and converted to the standard PDS format for public release. In addition, the Geospatial Data Abstraction Library (GDAL) is used to derive a terrain-shaded relief map, a color-shaded relief map, and a color slope map from the DTM as 8-bit GeoTIFFs [13].

Uncertainty Analysis: Qualitative and quantitative uncertainty analysis is performed for every NAC DTM and both the relative and absolute accuracies are reported.

Relative. Relative linear error (the one-dimensional error for elevation of one point with respect to another point, defined by the normal distribution function at 90% probability) as calculated by SOCET SET is recorded for each DTM as a measure of precision [8,10]. Precision is expected to be less than the DTM's GSD. The DTM horizontal precision is equal to the spatial sampling of the DTM [8].

Absolute. Every completed NAC DTM is compared to LOLA tracks, and the root mean square error (RMSE) for the vertical offset is recorded. In addition, the final DTM is re-registered to the LOLA tracks for a final evaluation of absolute accuracy. To be considered accurate, the RMSE must be less than the pixel scale of the DTM. The offsets in latitude, longitude, and elevation also need to be within the uncertainties attributed to the LOLA data, allowing for the precision of the DTM (for DTMs registered after April 2013, offsets should be <10 m horizontal-

ly and 1 m in elevation). DTMs created prior to 2013 use an alternative, less-accurate registration technique; as a result, these DTMs may have systematic errors that are larger than LOLA uncertainties. We plan to reprocess any pre-2013 DTMs with unacceptable offsets to the more accurate framework.

Scientific Applications: As the highest resolution topographic resource of the lunar surface available, the NAC DTMs are useful for sampling the full range of surface parameters across the globe, as well as across DTM mosaics derived from multiple stereo observations to cover broad areas.

Surface Roughness. Surface roughness was characterized for representative lunar terrain types and landforms by computing slopes from NAC DTMs sampled across a range of pixel scales; DTMs in this study had native post spacing of 2, 3, or 5 m and were down-sampled using bilinear interpolation. We calculated slope on a pixel-by-pixel basis using a 3x3 sample grid (i.e. for a pixel scale of 5 m slope was computed across a 15×15 m area). We used the LROC mare boundary shapefile to designate a total of 112 globally distributed DTMs as either 'mare' (81 DTMS) or 'highland' (31 DTMs) [14]. We excluded anomalously rough topography, such as large Copernican craters, from this preliminary analysis.

The median, mean, and standard deviation of the slopes in each DTM were computed for each pixel scale. The means of these slope parameters were then computed separately for all the 'mare' (n=81) and 'highland' DTMs (n=31) (Table 1). For comparison, slopes at larger pixel scales (333 m and 500 m, or 1000 m and 1500 m baselines) were computed from the Global Lunar DTM 100m (GLD100), a product created from LROC WAC stereo observations that covers 98.2% of the lunar surface [15] (Table 1). The NAC DTMs show that future rovers should be designed to handle average terrains up to at least 11° for highland targets and up to at least 5° for mare targets.

***Table 1: NAC** Slope Statistics for Mare and Highlands*

	Highlands			Mare		
Pixel Scale (m)	Mean of Median	Mean of Means	Mean of St. Dev.	Mean of Median	Mean of Means	Mean of St. Dev.
2	9.6°	11.1°	7.4°	3.5°	4.9°	4.5°
5	9.1°	11.0°	7.0°	2.8°	3.9°	3.9°
10	8.9°	10.4°	6.8°	2.6°	3.9°	4.0°
25	8.6°	10.1°	6.8°	2.1°	3.2°	3.6°
50	8.3°	9.9°	6.7°	1.8°	3.0°	3.5°
100	8.0°	9.6°	6.6°	1.4°	2.4°	3.2°
250	7.3°	8.9°	6.4°	1.0°	1.5°	2.2°
333	5.8°	7.5°	6.0°	0.8°	1.2°	1.9°
500	5.6°	7.2°	5.9°	0.6°	1.1°	1.8°

DTM Mosaics. Many features on the Moon are larger than the NAC field-of-view (~5 km by 26 km from 50 km altitude), so complete topographic characterization requires multiple stereo pairs to build a regional DTM mosaic; such multiple stereo pair observations of key targets are frequently acquired and processed. One such target is a large lobate flow deposit (50.535°S, 291.713°E) 600 km southeast of the basin rim that we interpret as emplacement of Orientale ejecta (Fig. 1). High-resolution DTM coverage allows not only estimates of material volume moved and deposited, but also enables numerical modeling of emplacement conditions. The flow is characterized by a hummocky and generally horizontal upper surface, with steep and sharp margins where topographically unconfined (Fig. 1). The slope (calculated across a 15×15 m area from 5 m pixel scale DTM) of the margin scarp often is steeper than 30° and commonly >36°, indicating cohesive or coherent material. The area of the flow shown in Fig. 1 is ~350 km^2, and the relief above the surrounding terrain ranges from 300 m - 500 m, a volume of >100 km^3. The area of the DTM is <20% of the whole deposit; assuming the thickness is uniformly >300 m, the whole deposit represents >500 km^3 of ejected material. Complete stereo coverage of key targets within the Orientale ejecta field will enable a quantitative understanding of basin ejecta emplacement mechanisms applicable to the Moon and other terrestrial bodies.

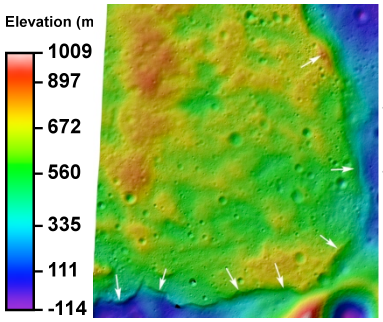

***Fig. 1:** Portion of Orientale lobate flow deposit. NAC DTM mosaic made from 6 stereo pairs (24 NAC images). White arrows indicate the extent of the flow.*

Production: As of January 2016, ASU has released 293 individual stereo pairs in 167 regions of interest, covering a total area of ~94,194 km^2. All associated products are released through the PDS every three months and are available at http://wms.lroc.asu.edu/lroc/rdr_product_select.

References: [1] Robinson, et al. (2010) *Space Sci. Rev., 150,* 81-124. [2] Mazarico, et al. (2013) *LPS XLIV*, Abs. #2414. [3] Anderson, et al. (2004) *LPS XXXV,* Abs. #2039. [4] Humm, et al. (2015) *Space Sci. Rev*., 1-43. [5] Acton (1996) *Planetary Space Sci., 44*. [6] Burns, et al. (2012) *ISPRS, XXXIX-B4,* 483-488. [7] Forstner, et al. (2013) *Manual of Photogrammetry (6th ed.),* 785-955. [8] BAE Systems (2009) *SOCET Set User Manual.* v. 5.5. [9] Speyerer, et al. (2012) *ELS.* [10] Zhang, (2006) *GeoCue Corp. 2nd Tech. Exchange Conf,* p. 32. [11] Zhang, et al. (2006) *ASPRS,* p. 12. [12] Miller, et al. (2013). *Manual of Photogrammetry (6th ed.),* 1009-1043. [13] Wamardam, (2008) *Open Source Approaches in Spatial Data Handling,* 87-108. [14] Nelson, et al. (2014) *LPS XLV*, Abs. #2861. [15] Scholten, et al. (2012), *J Geophys Res*, 117(E12).